Published in final edited form as:
Clin Cancer Res. 2021 March 15; 27(6): 1807–1820. doi:10.1158/1078-0432.CCR-20-3313.

Delta-24-RGD, an oncolytic adenovirus, increases survival and promotes proinflammatory immune landscape remodeling in models of AT/RT and CNS-PNET

Marc Garcia-Moure[#1,2,3,*], **Marisol Gonzalez-Huarriz**[#1,2,3], **Sara Labiano**[1,2,3], **Elizabeth Guruceaga**[1,4], **Eva Bandrés**[1,5], **Marta Zalacain**[1,2,3], **Lucía Marrodan**[1,2,3], **Carlos de Andrea**[1,6], **Maria Villalba**[1,6,7], **Naiara Martinez-Vélez**[1,2,3], **Virginia Laspidea**[1,2,3], **Montse Puigdelloses**[1,2,8], **Jaime Gallego Perez-Larraya**[1,2,8], **Ignacio Iñigo-Marco**[1,2,3], **Renata Stripecke**[9], **Jennifer A Chan**[10], **Eric H Raabe**[11,12], **Marcel Kool**[13,14,15], **Candelaria Gomez-Manzano**[16,17], **Juan Fueyo**[17,18], **Ana Patiño-García**[1,2,3], **Marta M Alonso**[1,2,3,*]

[1]Health Research Institute of Navarra (IdiSNA), Pamplona, Navarra, Spain

[2]Program in Solid Tumors, Foundation for the Applied Medical Research, Pamplona, Navarra, Spain

[3]Department of Pediatrics, Clínica Universidad de Navarra, Pamplona, Spain

[4]Bioinformatics Platform, Center for Applied Medical Research (CIMA), University of Navarra, Pamplona, Spain

[5]Immunology Unit, Hematology Department, Complejo Hospitalario de Navarra, Pamplona, Spain

[6]Department of Pathology, Clínica Universidad de Navarra, Pamplona, Spain

[7]Centro de Investigación Biomédica en Red de Cáncer (CIBERONC), Madrid, Spain

[8]Department of Neurology, Clínica Universidad de Navarra, Pamplona, Spain

[9]Department of Hematology, Hemostasis, Oncology and Stem Cell Transplantation; Laboratory of Regenerative Immune Therapies Applied of the Research Network REBIRTH; German Centre for Infection Research (DZIF), partner site Hannover, Hannover, Germany

[10]Department of Pathology and Laboratory Medicine, University of Calgary, Calgary, Alberta, Canada

[*]To whom correspondence should be addressed: mgmoure@unav.es; mmalonso@unav.es.

Author contributions:
Conception and design: MGM, MGH, and MMA
Development of methodology: All authors
Acquisition of data (provided animals, acquired and managed patients, provided facilities, etc.): All authors
Analysis and interpretation of the data (e.g., statistical analysis, biostatistics, and computational analysis): MGM, MGH, EG, SL, APG, JF, MK, CGM and MMA
Writing, review, and/or revision of the manuscript: All authors
Administrative, technical, or material support (i.e., reporting or organizing data and constructing databases): All authors
Study supervision: MGM and MMA

Conflict of interest: C. Gomez-Manzano and J. Fueyo report ownership interests (including patents) in and are consultants for DNAtrix. MMA has a research grant from DNAtrix. The remaining authors do not have potential conflicts of interest to disclose.

Europe PMC Funders Author Manuscripts

[11]Department of Pathology, The Johns Hopkins University School of Medicine, Baltimore, MD, USA

[12]Division of Pediatric Oncology, The Johns Hopkins University School of Medicine, Baltimore, MD, US

[13]Division of Pediatric Neurooncology, German Cancer Research Center (DKFZ) and German Cancer Consortium (DKTK), 69120 Heidelberg, Germany

[14]Hopp Children's Cancer Center (KITZ), Heidelberg, Germany

[15]Princess Máxima Center for Pediatric Oncology, Utrecht, the Netherlands

[16]Department of NeuroOncology, The University of Texas MD Anderson Cancer Center, Houston, Texas, USA

[17]Department of Genetics, The University of Texas MD Anderson Cancer Center, Houston, Texas, USA

[18]Department of Neurosurgery, The University of Texas MD Anderson Cancer Center, Houston, Texas, USA

[#] These authors contributed equally to this work.

Abstract

Purpose—Atypical teratoid/rhabdoid tumors (AT/RTs) and primitive neuroectodermal tumors (CNS-PNETs) are pediatric brain tumors with poor survival and life-long negative side effects. Here, the aim was to characterize the efficacy and safety of the oncolytic adenovirus Delta-24-RGDs, which selectively replicates in and kills tumor cells.

Experimental design—Delta-24-RGD determinants for infection and replication were evaluated in patient expression data sets. Viral replication and cytotoxicity were assessed *in vitro* in a battery of CNS-PNET and AT/RT cell lines. *In vivo*, efficacy was determined in different orthotopic mouse models, including early and established tumor models, a disseminated AT/RT lesion model and immunocompetent humanized mouse models (hCD34+-NSG-SGM3).

Results—Delta-24-RGD infected and replicated efficiently in all the cell lines tested. In addition, the virus induced dose-dependent cytotoxicity (IC_{50} below 1 PFU/cell) and the release of immunogenic markers. *In vivo*, a single intratumoral Delta-24-RGD injection (10^7 or 10^8 PFU) significantly increased survival and led to long-term survival in AT/RT and PNET models. Delta-24-RGD hindered the dissemination of AT/RTs and increased survival, leading to 70% of long-term survivors. Of relevance, viral administration to established tumor masses (30 days after engraftment) showed therapeutic benefit. In humanized immunocompetent models, Delta-24-RGD significantly extended the survival of mice bearing AT/RTs or PNETs (ranging from 11 to 27 days) and did not display any toxicity associated with inflammation. Immunophenotyping of Delta-24-RGD-treated tumors revealed increased CD8+ T cell infiltration.

Conclusions—Delta-24-RGD is a feasible therapeutic option for AT/RTs and CNS-PNETs. This work constitutes the basis for potential translation to the clinical setting

Keywords

AT/RT; CNS-PNET; Delta-24-RGD; virotherapy; immunotherapy

Europe PMC Funders Author Manuscripts

Introduction

Brain tumors are the solid tumors most frequently affecting children under 15 years old and have a devastating impact on childhood mortality, as they contribute to nearly 30% of all cancer deaths in children (1). By histological grouping, embryonal tumors comprise up to 24.9% of central nervous system (CNS) malignancies in infants under one year old, as well as 20.2% of those in children 1–4 years old (2). Embryonal CNS tumors include a heterogeneous group of highly cellular and mitotically active immature-appearing neoplasms that are able to invade surrounding tissues and disseminate through the cerebrospinal fluid (CSF) (3,4). Among these embryonal CNS tumors, in the present study, atypical teratoid/rhabdoid tumors (AT/RTs) and CNS primitive neuroectodermal tumors (CNS-PNETs), two aggressive brain tumors that comprise nearly 30% of embryonal tumors in children, were the focus (1).

AT/RTs are highly malignant brain tumors that are characterized by biallelic loss of function of SWI/SNF-related matrix-associated actin-dependent regulator of chromatin subfamily b-member 1 (SMARCB1) or, more rarely, SMARCA4 (5–7). AT/RT peak incidence occurs during the first two years of life and represents the most common type of malignant CNS tumor in children under one year old (2,8,9). Despite intensive multimodal therapies, most AT/RT patients inevitably experience recurrence, with a median survival time of 6–11 months (10,11). Unlike AT/RTs, CNS-PNETs represent a group of heterogeneous diseases, as revealed by molecular profiling. While researchers are still exploring molecular markers to precisely classify these tumors, the World Health Organization (WHO) has reclassified tumors that were previously defined as CNS-PNETs into a new group known as CNS-embryonal tumors, not otherwise specified (NOS) (12). Currently, most PNETs are treated with multimodal therapeutic protocols designed for high-risk medulloblastomas (13,14), which induce serious side effects in these patients. The prognosis of patients affected by these embryonal tumors remains dismal; therefore, it is essential to further explore novel therapeutic approaches to improve the life expectancy and quality of life of these children.

Oncolytic virotherapy is a promising therapeutic strategy based on the administration of cancer-selective viruses (15). Delta-24-RGD is a conditionally replicative adenovirus that contains two modifications that endow it with tumor specificity (16,17). Delta-24-RGD has shown promising therapeutic results in preclinical studies (17–20), leading to clinical trials for the treatment of ovarian cancer (21) and recurrent high-grade gliomas (*NCT00805376* and *NCT01956734*) (22). Previous results have revealed that intratumoral injection of Delta-24-RGD induces an initial phase of oncolysis, followed by a delayed inflammatory response with a reduction in the tumor burden (21,23). Importantly, an ongoing clinical trial employing Delta-24-RGD as a therapeutic agent in children affected by diffuse intrinsic pontine gliomas (*NCT03178032*) (24,25) has shown no signs of toxicity, thus underscoring the feasibility of Delta-24-RGD for the treatment of pediatric brain tumors.

Europe PMC Funders Author Manuscripts

In the present study, we explored the use of the oncolytic adenovirus Delta-24-RGD as a therapeutic agent in preclinical models of AT/RTs and CNS-PNETs *in vitro* and *in vivo*. We found that Delta-24-RGD replicated in and induced immunogenic cell death (ICD) marker expression in AT/RT and PNET cultures *in vitro*. Furthermore, *in vivo*, Delta-24-RGD treatment resulted in extended overall survival in several murine models of these diseases. Moreover, Delta-24-RGD treatment exerted significant antitumor effects on a metastatic model of AT/RTs. Delta-24-RGD treatment of immunocompetent humanized mouse models bearing AT/RTs or PNETs also led to an increase in overall survival and triggered antitumor immune responses that involved tumor immune microenvironment remodeling. Taken together, these results underscore the therapeutic potential of Delta-24-RGD for treatment of local and metastatic AT/RTs and PNETs and provide a foundation for the use of Delta-24-RGD in future clinical trials targeting these embryonal tumors.

Materials and methods

Bioinformatic analyses

The public datasets used for this analysis were downloaded from the Gene Expression Omnibus (GEO) data repository (http://www.ncbi.nlm.nih.gov/geo) (RRID:SCR_005012). For PNET and normal brain samples, the normalized data matrix for GSE14295 experiments was downloaded. Raw data for AT/RT samples (GSE70678) were also downloaded and normalized using RMA (26). First, a filtering process was performed in R/Bioconductor (27). Genes with expression levels lower than the noise signal in more than 50% of the samples of all the studied conditions (fetal brains, adult brains, PNETs, and AT/RTs) were considered to be not expressed. Then, the relative expression abundance was calculated for each gene by gene expression standardization with a mean of 0 and a standard deviation of 1.

Infectivity assays

A total of $2x10^5$ cells (six-well plates) were infected with Delta-24-RGD/GFP at a multiplicity of infections (MOI) of 0, 0.1, 1, 10, or 100 plaque-forming units (PFUs)/cell. At 48 h postinfection, transduction was verified by fluorescence microscopy, after which samples were harvested and washed with phosphate-buffered saline (PBS). Then, the percentage of GFP+ cells was determined by flow cytometry (FACSCantoII) and analyzed with FlowJo V10 (BD Biosciences, RRID:SCR_008520).

Activity of the transcription factor E2F1

A total of $3x10^5$ cells (24-well plates) were transfected (Fugene 6; E2691; Promega) with 250 ng of plasmid E2F1-Luc expressing a firefly luciferase reporter under the control of an E2F1-responsive promoter (28). Additionally, 250 ng of pRL-CMV, which constitutively expresses *Renilla* luciferase (E2261; Promega), was cotransfected as a transfection control. Twenty-four hours later, firefly and *Renilla* luciferase activities were measured using a Dual-Luciferase Reporter Assay System according to the manufacturer's instructions (E1910; Promega).

Viral proteins

A total of $2x10^5$ PNET or AT/RT cells (six-well plates) were infected with Delta-24-RGD at an MOI of 0, 5, 10, 25, or 50 PFUs/cell. At 16 h postinfection, the cultures were washed with PBS, and fresh growth medium was added. At 48 h postinfection, the cells were harvested and washed with PBS. Proteins were extracted with PBS-0.1% SDS, and protein concentrations were measured with Protein Assay Dye Reagent (Bio-Rad Laboratories (RRID:SCR_008426). Then, the presence of viral proteins (E1A and fiber) was detected by Western blotting (see the supplementary materials for the detailed protocol).

Viral replication assays

Cell cultures (10^5 cells per well; six-well plates) were infected with 10 PFUs/cell of Delta-24-RGD. After 72 h, complete cell cultures were collected and freeze-thawed three times, and total infectious titers were determined by serial dilutions in HEK293 cells by hexon staining (29).

Cell viability assays

Adherent cell lines were established as follows. We performed three-day and five-day kinetic studies to establish the most appropriate number of cells per 96-well plate, which were as follows: BT-12, HB, and PFSK-1: 2000 cells; CHLA-266: 6000 cells; and CHLA-06: 15000 cells. Then, cultures were infected with Delta-24-RGD at different MOIs ranging from 0 to 50. Cell viability was measured three and five days later using the CellTiter 96 Aqueous One Solution Cell Proliferation Assay (G3581; Promega), as previously described (30).

Suspension cell lines were established as follows. Both CTX and BT-183 cells grown in suspension were plated at a density of $2x10^5$ cells per well in six-well plates. At three and five days after infection with the same doses as above, cells were stained with trypan blue to enable cell counting. Dose-response curves were analyzed using GraphPad Prism 8 (Statistical Software for Sciences, RRID:SCR_002798) to determine the IC_{50} of Delta-24-RGD in these cells.

Measurement of DAMPs

Each cell line was plated at a density of $2x10^5$ cells per well (six-well plates) and infected with Delta-24-RGD at the corresponding three-day IC_{50}. Seventy-two hours later, the concentrations of the damage-associated molecular pattern (DAMP) markers Hsp90α (ADI-EKS-895; Enzo Life Sciences Inc.), HMGB1 (ST51011; IBL International), and ATP (ENLITEN ATP Assay System; FF2000; Promega) were measured in supernatants of infected and mock-infected cultures.

Calreticulin (CRT) translocation to the plasma membrane was determined by immunofluorescence staining of $2x10^4$ cells infected with Delta-24-RGD at a dose corresponding to the three-day IC_{50} (or PBS as a negative control). At 4 h postinfection, cells were fixed in 4% methanol-free formaldehyde (28906; Thermo Fisher Scientific) for 15 min at 37°C and then stained with appropriate antibodies. The extended immunofluorescence protocol is included in the supplementary materials.

Animal procedures and in vivo tumor models

In vivo experiments with PFSK-1 and JHU-HB-GBMP1 tumor xenograft models were carried out in 4- to 6-week-old female athymic nude (nu/nu) mice (Envigo). Studies of BT-183, BT-12, CHLA-06, and CHLA-266 xenograft models were performed in 4- to 6-week-old Balb/c-Rag2tFwa-Il2rg mice. In addition, hCD34-humanized mice (hu-CD34-NSG-SGM3; The Jackson Laboratory) were used to develop supratentorial PFSK-1 (10^5 cells) and CHLA-06 ($2x10^6$ cells) tumors in an immunocompetent environment.

Tumor cells and treatments were injected following the guide-screw system described by Lal et al. (31). For the orthotopic supratentorial model, CHLA-266 ($2x10^6$ cells), PFSK-1 (10^5 cells), or JHU-HB-GBMP1 (10^6 cells) cells were injected into the striatum at the following coordinates with respect to the bregma: 2.5 mm lateral, 1 mm cranial, and 2 mm deep (3.5 mm including screw height). The infratentorial xenograft model was established by injecting $5×10^5$ tumor cells (BT-12, CHLA-06, or CHLA-266) into the cerebellum 1 mm lateral, 0.8 mm posterior, and 2 mm deep (3.5 mm including screw height) with respect to lambda. The disseminated model that we used was based on the intraventricular administration procedure described by Studebaker et al. (32). For this model, BT-12-GFP/luc (10^6 cells) cells were injected into the right lateral ventricle at 1 mm lateral, 0.5 mm posterior, and 3.2 mm deep with respect to the bregma. Mice were screened via bioimaging prior to being treated and were withdrawn in cases in which no reporter signal was detected at the ventricle.

Intratumoral treatments were carried out by injecting 3 μL of PBS or Delta-24-RGD following the same guide-screw system at the coordinates of the corresponding tumor model. In survival experiments, mice were euthanized when symptoms of disease (e.g., loss of weight, hunched position) were evident. A summary of the in vivo experiments performed is located in Table S1.

Ethical approval for all animal studies was granted by the Animal Ethical Committee of the University of Navarra (CEEA) under the protocols CEEA/091-18, CEEA/094-15, and CEEA/066-18. All animal studies were performed at the veterinary facilities of the Center for Applied Medical Research in accordance with institutional, regional, and national laws and ethical guidelines for experimental animal care.

Histological staining

Formalin-fixed paraffin-embedded (FFPE) brain sections (4-μm thickness) were stained by the hematoxylin/eosin method or were immunostained as follows: anti-hexon (1:2000; AB1056; Merck Millipore), anti-E1A (1:1000, sc-430; Santa Cruz; CA; USA), anti-CD3 (1:300; RM9107; Thermo Fisher), anti-Iba-1 (1:4000; 019-19741; Wako), and anti-GFP (1:1000; ab6556; Abcam). Signals were developed with Vectastain ABC kits (Vector Laboratories Inc.) according to the manufacturer's instructions.

Multiplexed immunofluorescence

A multiplex immunolabeling protocol based on tyramide signal amplification (TSA) and Opal fluorophores was developed and validated essentially as described previously (33). Single-plex chromogenic immunohistochemistry assays were used as the gold standard for

cell antigen visualization and compared against the corresponding fluorescent channel for multiplexed immunofluorescence on sequential FFPE sections. An extended explanation is included in the supplementary materials.

Tissue imaging, spectral unmixing, and phenotyping

Multiplexed immunofluorescence slides were scanned on a Vectra-Polaris Automated Quantitative Pathology Imaging System (Akoya Biosciences), as described previously (33,34). An extended explanation is included in the supplementary materials.

Statistical analyses

Statistical analyses were performed using GraphPad Prism 8 (Statistical Software for Sciences). Dose-response curves for infectivity and viability were obtained by nonlinear regression. For quantitative variables, data with normal distributions were assessed by Shapiro-Wilk tests, and then comparisons among groups were performed using two-tailed (one-tailed when indicated) nonparametric tests with 95% confidence intervals for data sets that were nonnormally distributed (Mann-Whitney or Kruskal-Wallis tests) or parametric tests when normality was confirmed (Student's t-test or one/two-way ANOVA). Dunn's (nonparametric) or Dunnett/Tukey's (one- and two-way ANOVA, respectively) corrections were applied for *post hoc* pairwise comparisons. Kaplan-Meier plots were analyzed by log-rank (Mantel-Cox) tests.

Results

AT/RT and PNET cultures are permissive to Delta-24-RGD infection in vitro

Since infection by Delta-24-RGD is mediated by integrins and coxsackie and adenovirus receptor (CAR) (16,35,36), we first assessed the relative expression levels of α_v integrin (ITGAV), β_3 integrin (ITGB3), β_5 integrin (ITGB5), and CAR (CXADR) *in silico* in AT/RT and PNET samples, as well as in normal fetal and adult brain samples (Figure 1A). The expression levels of α_v integrins and CAR were observed in both AT/RT and PNET samples, and their relative abundances were above the mean expression of their respective transcriptomes. In contrast, normal fetal brain samples showed lower relative mRNA expression of α_v-integrin. In terms of the β_5-integrin and β_3-integrin genes, their relative abundances in PNET samples were similar to those in normal brain samples and were lower than those in AT/RT samples. We obtained similar results when we performed analyses that accounted for the different molecular subgroups of AT/RTs (Figure S1A). Collectively, these *in silico* findings revealed that AT/RTs and PNETs express receptors for Delta-24-RGD. Confirming the potential susceptibilities of AT/RTs and PNETs to Delta-24-RGD infection, AT/RT and PNET cell lines displayed robust CAR and integrin-β_5 expression levels (Figure 1B). In accordance with the gene expression of β_3 integrin in tumor samples, this receptor was nearly absent in the four cell lines evaluated. Finally, to determine whether the expression of these viral receptors enables endocytosis of the oncolytic virus Delta-24-RGD, AT/RT and PNET cell lines were infected with Delta-24-RGD expressing the reporter GFP at increasing MOIs ranging from 0.1–100 PFUs/cell. We observed dose-dependent expression of GFP in AT/RT and PNET cultures (Figure 1C). More than 80% of AT/RT and PNET cells were infected at an MOI of 1, and virtually 100%

infection was achieved with an MOI of 10 (Figure 1D). In fact, cells infected at a MOI of 100 were already detached and dying at 48 h (Figure 1C). The MOI needed to yield a 50% infection rate was below 0.1 PFUs/cell for BT-12 and CHLA-06 cells, 0.18 PFUs/cell for CHLA-266 cells, and 0.23 PFUs/cells for PFSK-1 cells (Figure 1D).

Since the heterogeneity and scarcity of CNS-PNET models are major drawbacks for conducting preclinical studies, we next studied the oncolytic effects of Delta-24-RGD on other "PNET-like" tumors to cover a broader range of embryonal tumors, excluding medulloblastomas. Therefore, we assessed the expression levels of viral receptors in the BT-183 cell line, which was derived from an embryonal tumor with multilayered rosettes (ETMRs) (37), and the JHU-CTX-GBMP1 (CTX) and JHU-HB-GBMP1 (HB) cell lines, which correspond to models of glioblastomas (GBMs) with PNET-like components (i.e., currently known as glioblastomas with primitive neuronal components). CAR expression was detected in the ETMR cell line BT-183 (Figure S1B), as well as in GBM-PNET-like cultures (Figure S1B). Similar to our results for AT/RT and PNET cultures, the expression levels of $\alpha_v\beta_3$ integrin in ETMR cells and GBM-PNET-like cells were negligible, while $\alpha_v\beta_5$ integrin was detected in the three cell lines tested. Overall, the expression of adenoviral receptors was lower in these models, which is in agreement with their higher resistance to adenoviral infection (Figure S1C). According to these data, we concluded that AT/RT and PNET cell lines could be readily infected by Delta-24-RGD.

Delta-24-RGD replicates in and exerts antitumor activity in AT/RT and PNET cultures in vitro

Delta-24-RGD replication in tumor cells requires a constitutively active E2F pathway. Compared to those in normal human adult and fetal brain samples, the relative E2F-1 levels in PNET and AT/RT samples were higher, indicating that these tumor cells may be permissive to Delta-24-RGD replication (Figure 2A). The expression levels of other positive cell cycle regulators, such as *CCND1* and *CDK4*/6, were enriched in different AT/RT molecular subgroups (Figure S2A). In addition, AT/RT cell lines displayed deletion of the tumor suppressor gene *SMARCB1* (Table S2), and the PFSK-1 cell line harbored p53 mutations; both aberrations resulted in cell cycle deregulation. Regarding direct alterations in the pRb-E2F pathway, only BT-12 cells showed loss of the *CDKN2A* and *CDKN2B* genes encoding the CDK4/6 inhibitors $p16^{INK4a}$ and $p15^{INK4b}$, respectively. Corroborating this finding, we found a significant increase in E2F-1 promoter activity in PNET and AT/RT cell lines compared with normal astrocytes (Figure 2B). This result demonstrates that although the pRb-E2F pathway is not directly affected at the genomic level in some tumors, other epigenetic mechanisms may upregulate E2F-1 activation, thus suggesting that these tumor cells are potential targets for Delta-24-RGD replication.

We next assessed viral cycle progression in AT/RT and PNET cultures. The E1A protein, which is an adenoviral protein that is transcribed immediately after infection, was detected in all infected AT/RT and PNET cultures at 16 and 48 h after infection (Figure S2B). Similarly, fiber, a protein that is expressed after viral genome replication, was detected at 48 h but not at 16 h after infection (Figure S2B). The viral titers in all infected AT/RT and PNET cultures were significantly increased at 72 h after infection (Figures 2C and S2C).

These results confirm that Delta-24-RGD undergoes a replicative cycle in AT/RT, PNET, and PNET-like cells, although the viral burst size is dependent on the specific cellular model.

Next, we assessed the antitumor effects of Delta-24-RGD on these *in vitro* models (Figures 2D and S2D). Dose-dependent cytolysis was observed at three days after infection in all cultures, which was in agreement with the generation of infectious viral particles observed at 72 h after infection. At five days postinfection, the initial dose required to reach cell death in 50% of a culture dropped dramatically to 1.0 PFUs/cell or less due to the increase in infection/replication/cytolysis rounds.

In addition to its cytolytic activity, Delta-24-RGD also promotes a proinflammatory environment at tumor sites by boosting antitumor immune responses (20,22). One of the mechanisms that participates in the enhancement of immune responses is the secretion of DAMPs into the extracellular medium by infected tumor cells. We observed significant increases in secreted DAMPs Hsp90α and HMGB1 levels following Delta-24-RGD infection in comparison to mock infection in all tested cell lines (Figure 2E). In contrast, Delta-24-RGD infection did not significantly alter ATP concentrations in any cell line. Translocation of the endoplasmic reticulum-resident protein calreticulin (CRT) to the cell surface of tumor cells is another well-known mechanism that contributes to the immunogenicity of tumor cells by acting as an “eat-me” signal to promote tumor cell phagocytosis by macrophages (38). Early Delta-24-RGD infection triggered translocation of CRT to the plasma membrane (Figure 2F). Thus, we concluded that Delta-24-RGD induces antitumor effects *in vitro*.

Administration of Delta-24-RGD extends the overall survival of early and advanced PNET and AT/RT mouse models

Next, we investigated the therapeutic potential of Delta-24-RGD in mouse models of PNETs and AT/RTs. To this end, mice bearing orthotopically injected PFSK-1 cells were treated with a single intratumoral injection of Delta-24-RGD (10^7 or 10^8 PFUs/mouse) or PBS (mock-treated group). The mice treated with the lowest dose of Delta-24-RGD did not show a significant increase in median survival; however, this treatment yielded 22% long-term survivors (two out of nine mice) free of disease. The mice treated with the highest dose of Delta-24-RGD showed a significant increase in median survival, and 56% of the mice were long-term survivors (Figure 3A). The long-term survivors were euthanized on day 97 after infection, and no visible tumor lesions were detected via hematoxylin/eosin staining (Figure S3A). Histological analyses performed at 14 days after injection revealed the presence of highly vascularized tumor masses spanning most of the right brain hemisphere in mock-treated mice. E1A and hexon staining in Delta-24-RGD-treated mice demonstrated *in vivo* infection and replication, respectively (Figure 3B). Furthermore, activated microglia were found at a high density at the tumor edge, labeled with the marker Iba-1, and indicated tumor infiltration by reactive amoeboid microglia, which was in contrast with the resting microglia (stellate shape) present in most of the normal parenchyma (Figure 3B). In addition, in Delta-24-RGD-treated mice, the highest degree of tumor infiltration by microglia was detected in areas that matched the infected areas, thus indicating that

the virus induced substantial changes in the immune landscape surrounding the tumor microenvironment.

To determine whether the efficacy of this virus may be relevant to a broad range of different types of tumors *in vivo*, we next assessed the effects of Delta-24-RGD on PNET-like mouse models with primitive features such as ETMRs and GBMs with PNET-like components. E1A and hexon staining confirmed that Delta-24-RGD infected and replicated in ETMR-induced tumors (BT-183 cell lines, Figure S3B). However, unlike in mice with PFSK-1 cell-induced PNET tumors, ETMRs showed no effects of treatment with Delta-24-RGD on tumor growth or infiltration of Iba-1-positive cells (microglia/macrophages). Unexpectedly, although replication of Delta-24-RGD was observed both *in vitro* and *in vivo*, survival curve comparisons showed no therapeutic benefit of Delta-24-RGD at the doses used to treat ETMR-induced tumors in mice (Figure S3C). Similar experiments were performed with the GBM PNET-like cell line HB. Histological analyses of HB tumors at 14 days after Delta-24-RGD treatment showed the presence of E1A and hexon proteins at the tumor site in the Delta-24-RGD-treated mice (Figure S3D). In this model, mice treated with the highest Delta-24-RGD dose displayed a significant increase in overall survival compared with mock-treated mice (Figure S3E).

Next, we assessed the antitumor effects of Delta-24RGD on several AT/RT infratentorial models (CHLA-06, BT-12 and CHL-266 cells) following the protocol described above. At the highest dose, Delta-24-RGD treatment led to significant increases in median survival and long-term survival in the three models. The increase in median survival ranged from 10 days for CHL-06 tumors to 45 days for BT-12 and CHLA-266 tumors (Figure 3C). The lowest dose tested also showed a significant improvement in the median survival of mice bearing CHL-06 tumors (13.5-day increase). Delta-24-RGD infection and replication were detected in tumor masses by E1A and hexon staining, respectively. Similar to PFSK-1 tumors, CHLA-06 tumors treated with Delta-24-RGD showed accumulation of microglia at the tumor rim and infiltration of reactive microglia, which were exacerbated in the Delta-24-RGD-containing regions of the tumors (Figure 3D). Furthermore, the presence of the adenoviral proteins E1A and hexon was detected in tumor masses nearly 100 days after injection of Delta-24-RGD (Figure S4A and S4B), indicating that replication of the virus lasted as long as the time course of tumor cell propagation.

Because AT/RTs can also arise at supratentorial locations, CHLA-266 cells were engrafted orthotopically in the striatum (Figure 3E). In this model, we observed a significant increase in the median survival of Delta-24-RGD-treated mice (39 days), and 29% of these mice (two out of seven) were long-term survivors with no symptoms of disease. These data underscore the therapeutic benefit of Delta-24-RGD in preclinical mouse models of localized AT/RTs *in vivo*.

Next, we addressed whether treatment with Delta-24-RGD could be effective in established tumors, which better recapitulate clinical conditions in human patients. Thus, we first established the time frames in which mice bearing PFSK-1 or CHLA-266 cells (supratentorial PNET and AT/RT models, respectively), as well as those bearing CHLA-06 cells (infratentorial AT/RT model), displayed visible tumors (Figure S4C). PFSK-1 and

Europe PMC Funders Author Manuscripts

CHLA-06 tumor-bearing mice were treated seven and eight days after cell implantation, respectively, while treatment of CHLA-266 tumor-bearing mice was delayed to 29 days. Of importance, Delta-24-RGD treatment at the highest dose resulted in a significant increase in survival and led to long-term survival in the three models assessed. Moreover, the lowest dose also showed a significant benefit in the PFSK-1 and CHL266 models (Figure 3F). Anatomopathological analysis showed the capacity of the virus to spread through the tumors (Figure S4D). In addition, these analyses revealed ongoing infection and replication in the tumor mass (E1A and hexon staining, respectively), as well as a high degree of reactive microglial infiltration (Figure S4E). Furthermore, we observed an enrichment of reactive microglia at viral replication foci. These data indicate that virus treatment results in microglial activation.

Delta-24-RGD treatment hinders the development of disseminated AT/RT lesions in preclinical mouse models

Because the presence of disseminated disease is a major hurdle in the efficacy of antitumor therapies in AT/RT patients (39), we next evaluated the efficacy of Delta-24-RGD in a preclinical mouse model of this condition. Luminometry and histology in pilot studies confirmed that the BT-12 cell line was able to generate disseminated lesions upon intraventricular injection, as we observed luciferase signals at distal regions in the spinal cord and the presence of extracranial tumor lesions (Figure 4A). *In vivo* experiments showed that by day 26, 58% of mock-treated mice developed secondary tumors (Figure 4B). Bioluminescence images captured at early stages (days 11 and 22) revealed that Delta-24-treated mice displayed a significantly lower tumor burden than mock-treated mice (Figure 4C, 4D, 4E). Regarding the efficacy of Delta-24-RGD in this disseminated model, administration of the lower dose (10^7 PFUs) increased median survival by 21.5 days and produced two long-term survivor animals; however, the difference was not significant. In contrast, treatment with the highest Delta-24-RGD dose (10^8 PFUs) significantly increased median survival compared to PBS treatment mice and led to 70% of the mice becoming long-term survivors (Figure 4F). Anatomopathological analysis of the spinal cord of long-term survivors revealed that they were free of disease (Figure S4F). These data underscore the antitumor effect of Delta-24-RGD even in the context of disseminated disease.

Delta-24-RGD induces an antitumor immune response in humanized PNET and AT/RT models

Previous preclinical and clinical data have provided evidence that Delta-24-RGD enhances the antitumor immune response in brain tumors (20,22,40). Therefore, we evaluated the effects of Delta-24-RGD in an immunocompetent background using NSG-SMG3 mice humanized with hCD34+ progenitor cells that recapitulate both the innate and adaptive branches of the immune system (41). Human leukocyte antigen (HLA) typing was performed in PNET and AT/RT cell lines with the aim of choosing a donor with at least HLA-A matching (Supplementary Materials).

Survival studies demonstrated that treatment of mice bearing PFSK-1 or CHLA-06 cells with a single injection of Delta-24-RGD (10^8 PFUs) resulted in a significant increase in overall survival compared to mock treatment (28 vs 55 days for PFSK-1 cells and 23 vs 34

days for CHLA-06 cells) (Figure 5A and 5B). Moreover, one animal survived the PFSK-1 challenge at the end of the study (Figure 5A). Assessment of mouse body weight throughout the experiment revealed no signs of toxicity associated with virus-mediated inflammation induced by Delta-24-RGD (Figure S5A).

Histological analyses of brain samples from CHLA-06 tumor-bearing mice indicated ongoing viral infection and replication in Delta-24-RGD-treated mice (Figure 5C). Multispectral immunofluorescence panels of different immune populations revealed that most immune cells accumulated in the tumor-invasive margin (Figures 5C and S5B) and in Delta-24-RGD-containing regions (Figure 5C). In both Delta-24-RGD-treated mice and mock-treated mice, the presence of CD20+ B cells was nearly negligible (Figure 5D). Furthermore, Delta-24-RGD also induced reductions in the frequency of CD68+ cells (macrophages) in the tumor and at the invasive margin, although the reduction was less pronounced at the latter site. No differences were observed in terms of the total CD11b+ myeloid population, although the antibody that was used also detects the murine orthologue; thus, this particular assessment may have been hampered by the high abundance of mouse microglia. Interestingly, even though no differences were observed between the groups in regard to total T cells (CD3+), there was a remarkable increase in the CD8+ subpopulation in the Delta-24-RGD-treated group, which was nearly absent in the mock-treated group. To validate our results, the multispectral immunofluorescence results were confirmed by conventional immunohistochemistry (Figure S5C).

Surprisingly, PFSK-1 tumors showed no evidence of viral infection or T cell infiltration despite observation of clear therapeutic effects (Figure 5E). Nevertheless, analysis of the macrophage/microglial marker Iba-1 revealed pronounced activation and recruitment of these cells at the tumor margin in Delta-24-RGD-treated mice.

Finally, survival experiments were performed for an ETMR model (BT-183) established with humanized mice. However, although no signs of toxicity were observed (Figure S5D), Delta-24-RGD showed no therapeutic benefit (Figure S5E), and there was no T cell infiltration despite evidence of replication of Delta-24-RGD (Figure S5F).

Although the outcomes of the different models were variable, these results are encouraging and may reflect the heterogeneity of the type of tumor, donor and immune response (T cell responses versus predominant macrophage activation).

Discussion

Potential tumor targets of Delta-24-RGD must be permissive to viral infection and replication. We previously confirmed the expression of adenoviral receptors and the transcription factor E2F-1 in gene expression data sets from tumor biopsies (42,43), providing direct translational relevance. Unlike the common features of other brain tumors, canonical oncogenic mutations in components of the pRb-E2F pathway, such as *CDK4*/CCND1 amplification and *CDKN2A*/B deletion, are uncommon in CNS-PNETs (44,45) and are nearly absent in AT/RTs (46,47). Nonetheless, epigenetic deregulation mediated by loss

of SMARCB1 in AT/RTs, as well as loss of p53 and amplification of different tyrosine kinase (TKs), results in aberrant cell cycle progression that allows viral replication.

Although virotherapy has been evaluated in embryonal tumors, mainly medulloblastomas (48–51), there is a paucity of preclinical studies investigating these types of tumors. Nonetheless, an oncolytic measles virus was found to have therapeutic effects on localized and disseminated models of AT/RTs (52). Another oncolytic adenovirus, VCN-01 (armed with hyaluronidases), was demonstrated to be efficacious in a model of supratentorial PNETs (53). These previous findings together with our present results underscore the potential of virotherapies and the need to translate them to clinical trials.

Despite our use of immunodeficient mice in the present study, our *in vivo* models still developed immune responses in the myeloid compartments, and we observed that Delta-24-RGD triggered tumor infiltration of amoeboid reactive microglia, thus underscoring the ability of this virus to “warm” the tumor microenvironment to a proinflammatory status, which might contribute to enhancing antitumor immune responses (54). In our humanized mouse AT/RT model, we observed a decrease in the frequency of CD68+ cells after Delta-24-RGD treatment, which has been proposed to negatively impact the survival of patients with MYC-AT/RTs (55). Therefore, we speculate that Delta-24-RGD may have a direct effect on this population, inducing remodeling of the tumor microenvironment and stimulating the expansion and activity of CD8+ cytotoxic T lymphocytes (CTLs) to exert their antitumor effects. Interestingly, in the PFSK-1 humanized model, although we could not detect viral replication or T cell infiltration, we observed the existence of reactive glia. These data agree with a potential antitumor immune response. However, it might be that at 15 days, the immune response was already fading. In addition, we cannot rule out the possibility that other mechanisms were taking place (i.e., early innate response, cytotoxicity), and further studies are needed to test this hypothesis.

One of the limitations of our present study was the paucity of preclinical models. First, the availability of well-characterized human-derived CNS-PNET models is scarce; therefore, tumor models do not recapitulate the variability found in patients. Second, human adenoviruses do not exhibit high levels of replication in murine cells (56), so the oncolytic and immunostimulatory properties of Delta-24-RGD must be evaluated independently using human xenografts and syngeneic models, respectively (20). Transgenic mouse models have already been developed for spontaneous CNS-PNETs, AT/RTs, and ETMRs (57–59); however, these mice suffer from severe healthy conditions, and spontaneous tumor models are difficult to treat via intratumoral injections. The development of stable cell cultures from these tumors may be a desirable approach to overcome these difficulties. In the present study, we used humanized mice as an approach to evaluate the combined effects of viral replication and immunomodulation since such mice allow the study of xenografted human tumors in an immunocompetent environment. However, this model is per se complex and presents with intrinsic limitations, such as the age of the mice used in the analyses. Due to the engraftment process of human CD34+ cells, these mice are already adults by the time they can be used in experiments (approximately 15 weeks) and are therefore not an ideal model for trying to assess the immune system of children. Another important issue is the HLA matching of the immune system donor and tumor. Therefore, cautious should be

exerted when making definitive conclusions, and further studies are required to understand this process in depth.

In summary, we demonstrated that treatment with the oncolytic adenovirus Delta-24-RGD is a potential therapeutic approach for AT/RTs and PNETs. Our data showed that virus administration was safe and effective in controlling local, both supratentorial and infratentorial, advanced and disseminated tumors in models of AT/RTs and CNS-PNETs. These encouraging data open the door for oncolytic viruses to be considered serious candidates in the treatment of pediatric brain tumors and strongly support initiating clinical studies.

Supplementary Material

Refer to Web version on PubMed Central for supplementary material.

Acknowledgments

We thank Nature Authors Services for its linguistic assistance during the preparation of this manuscript.

Financial support

The performed work was supported through the Departamento de Salud del Gobierno de Navarra (54/2018-APG); Predoctoral Fellowship from Gobierno de Navarra (VL), Instituto de Salud Carlos III y Fondos Feder (PI19/01896 MMA, PI18/00164 APG); Amigos de la Universidad de Navarra (to MP); Fundación La Caixa/Caja Navarra (APG and MMA); Fundación El sueño de Vicky; Asociación Pablo Ugarte-FuerzaJulen (APG and MMA); and Department of Defense (DOD) Team Science Award under grant (CA 160525 MMA, CGM and JF). This project also received funding from the European Research Council (ERC) under the European Union's Horizon 2020 Research and Innovation Programme (817884 ViroPedTher to MMA).

Data and materials availability

The data and materials that support the findings of this study are available within the paper or Supplementary Information or available from the corresponding author upon request.

References

1. Ostrom, QT, Gittleman, H, Truitt, G, Boscia, A, Kruchko, C, Barnholtz-Sloan, JS. Neuro Oncol. Vol. 20. Oxford University Press; 2018. CBTRUS Statistical Report: Primary Brain and Other Central Nervous System Tumors Diagnosed in the United States in 2011-2015; iv1–86.
2. Ostrom, QT, de Blank, PM, Kruchko, C, Petersen, CM, Liao, P, Finlay, JL. , et al. Neuro Oncol. Vol. 16. Oxford University Press; 2015. Alex's Lemonade stand foundation infant and childhood primary brain and central nervous system tumors diagnosed in the United States in 2007-2011; x1–35.
3. Adekunle, M, Adesina, ATY. Phatology of embryonal tumors. medscape; 2018.
4. McGovern SL, Grosshans D, M A. Embryonal brain tumors. Cancer J. 2014; 20 (6) 397. [PubMed: 25415685]
5. Han, Kakkar A, Sarkar C, Julka, PramBiswas A, Kashyap LK. Atypical teratoid/rhabdoid tumors: Challenges and search for solutions. Cancer Manag Res. 2016; 8: 115–25. DOI: 10.2147/CMAR.S83472 [PubMed: 27695363]
6. Biegel, JA, Zhou, JY, Rorke, LB, Stenstrom, C, Wainwright, LM, Fogelgren, B. Cancer Res. Vol. 59. American Association for Cancer Research; 1999. Germ-line and acquired mutations of INI1 in atypical teratoid and rhabdoid tumors; 74–9.
7. Haberler C, Laggner U, Slavc I, Czech T, Ambros IM, Ambros PF, et al. Immunohistochemical Analysis of INI1 Protein in Malignant Pediatric CNS Tumors: Lack of INI1 in Atypical Teratoid/

Europe PMC Funders Author Manuscripts

Rhabdoid Tumors and in a Fraction of Primitive Neuroectodermal Tumors without Rhabdoid Phenotype. 2006. [PubMed: 17063089]

8. Biswas A, Kashyap L, Kakkar A, Sarkar C, Julka PK. Atypical teratoid/rhabdoid tumors: Challenges and search for solutions. Cancer Manag Res. 2016; 8: 115–25. [PubMed: 27695363]
9. Ostrom QT, Chen Y, De Blank PM, Ondracek A, Farah P, Gittleman H, et al. The descriptive epidemiology of atypical teratoid/rhabdoid tumors in the United States, 2001-2010. Neuro Oncol. 2014; 16: 1392–9. DOI: 10.1093/neuonc/nou090 [PubMed: 24847086]
10. Packer RJ, Biegel JA, Blaney S, Finlay J, Russell Geyer J, Heideman R, et al. Atypical Teratoid/Rhabdoid Tumor of the Central Nervous System: Report on Workshop. 2002. [PubMed: 12142780]
11. Gajjar A, Bowers DC, Karajannis MA, Leary S, Witt H, Gottardo NG. Pediatric brain tumors: Innovative genomic information is transforming the diagnostic and clinical landscape. J Clin Oncol. 2015; 33: 2986–98. DOI: 10.1200/JCO.2014.59.9217 [PubMed: 26304884]
12. Louis DN, Perry A, Reifenberger G, von Deimling A, Figarella-Branger D, Cavenee WK, et al. The 2016 World Health Organization Classification of Tumors of the Central Nervous System: a summary. Acta Neuropathol. 2016; 131: 803–20. [PubMed: 27157931]
13. Friedrich, C, von Bueren, AO, von Hoff, K, Gerber, NU, Ottensmeier, H, Deinlein, F. , et al. Neuro Oncol. Vol. 15. Oxford University Press; 2013. Treatment of young children with CNS-primitive neuroectodermal tumors/pineoblastomas in the prospective multicenter trial HIT 2000 using different chemotherapy regimens and radiotherapy; 224–34.
14. Jakacki RI, Burger PC, Kocak M, Boyett JM, Goldwein J, Mehta M, et al. Outcome and prognostic factors for children with supratentorial primitive neuroectodermal tumors treated with carboplatin during radiotherapy: A report from the Children's Oncology Group. Pediatr Blood Cancer. 2015; 62: 776–83. DOI: 10.1002/pbc.25405 [PubMed: 25704363]
15. Zhang, W-W. Cancer Gene Ther. Vol. 6. Nature Publishing Group; 1999. Development and application of adenoviral vectors for gene therapy of cancer; 113–38.
16. Rodriguez-Garcia A, Gimenez-Alejandre M, Rojas JJ, Moreno R, Bazan-Peregrino M, Cascallo M, et al. Safety and efficacy of VCN-01, an oncolytic adenovirus combining fiber HSG-binding domain replacement with RGD and hyaluronidase expression. Clin Cancer Res. 2014; Nov 14. 21: 1406–18. [PubMed: 25391696]
17. Fueyo J, Gomez-Manzano C, Alemany R, Lee PSY, McDonnell TJ, Mitlianga P, et al. A mutant oncolytic adenovirus targeting the Rb pathway produces anti-glioma effect in vivo. Oncogene. 2000; 19: 2–12. [PubMed: 10644974]
18. Dai, B, Roife, D, Kang, Y, Gumin, J, Rios Perez, MV, Li, X. , et al. Mol Cancer Ther. Vol. 16. American Association for Cancer Research; 2017. Preclinical Evaluation of Sequential Combination of Oncolytic Adenovirus Delta-24-RGD and Phosphatidylserine-Targeting Antibody in Pancreatic Ductal Adenocarcinoma; 662–70.
19. Garcia-Moure, M, Martinez-Vélez, N, Patiño-García, A, Alonso, MMM. J Bone Oncol. Vol. 9. Elsevier; 2017. Oncolytic adenoviruses as a therapeutic approach for osteosarcoma: A new hope; 41–7.
20. Martínez-Vélez, N, Garcia-Moure, M, Marigil, M, González-Huarriz, M, Puigdelloses, M, Gallego Pérez-Larraya, J. , et al. Nat Commun. Vol. 10. Nature Publishing Group; 2019. The oncolytic virus Delta-24-RGD elicits an antitumor effect in pediatric glioma and DIPG mouse models.
21. Kimball KJ, Preuss MA, Barnes MN, Wang M, Siegal GP, Wan W, et al. A phase I study of a tropism-modified conditionally replicative adenovirus for recurrent malignant gynecologic diseases. Clin Cancer Res. 2010; 16: 5277–87. DOI: 10.1158/1078-0432.CCR-10-0791 [PubMed: 20978148]
22. Lang FF, Conrad C, Gomez-Manzano C, Alfred Yung WK, Sawaya R, Weinberg JS, et al. Phase I study of DNX-2401 (delta-24-RGD) oncolytic adenovirus: replication and immunotherapeutic effects in recurrent malignant glioma. J Clin Oncol. 2018; 36: 1419–27. DOI: 10.1200/JCO.2017.75.8219 [PubMed: 29432077]
23. Lang, FF, Conrad, C, Gomez-Manzano, C, Tufaro, F, Yung, W, Sawaya, R. , et al. Neuro Oncol. Vol. 16. Oxford University Press; 2014. FIRST-IN-HUMAN PHASE I CLINICAL

Europe PMC Funders Author Manuscripts

TRIAL OF ONCOLYTIC DELTA-24-RGD (DNX-2401) WITH BIOLOGICAL ENDPOINTS: IMPLICATIONS FOR VIRO-IMMUNOTHERAPY; iii39

24. Tejada, S, Alonso, M, Patiño, A, Fueyo, J, Gomez-Manzano, C, Diez-Valle, R. Neurosurgery. Vol. 83. Oxford University Press; 2018. Phase I Trial of DNX-2401 for Diffuse Intrinsic Pontine Glioma Newly Diagnosed in Pediatric Patients; 1050–6.
25. Tejada, S, Díez-Valle, R, Domínguez, PD, Patiño-García, A, González-Huarriz, M, Fueyo, J. , et al. Front Oncol. Vol. 8. Frontiers; 2018. DNX-2401, an Oncolytic Virus, for the Treatment of Newly Diagnosed Diffuse Intrinsic Pontine Gliomas: A Case Report; 61
26. Irizarry RA, Bolstad BM, Collin F, Cope LM, Hobbs B, Speed TP. Summaries of Affymetrix GeneChip probe level data. Nucleic Acids Res. 2003; 31: e15. doi: 10.1093/nar/gng015 [PubMed: 12582260]
27. Gentleman, RC, Carey, VJ, Bates, DM, Bolstad, B, Dettling, M, Dudoit, S. , et al. Genome Biol. Vol. 5. BioMed Central; 2004. Bioconductor: open software development for computational biology and bioinformatics.
28. Alonso, MM, Cascallo, M, Gomez-Manzano, C, Jiang, H, Bekele, BN, Perez-Gimenez, A. , et al. Cancer Res. Vol. 67. American Association for Cancer Research; 2007. ICOVIR-5 shows E2F1 addiction and potent antiglioma effect in vivo; 8255–63.
29. Cascallo M, Gros A, Bayo N, Serrano T, Capella G, Alemany R. Deletion of VAI and VAII RNA Genes in the Design of Oncolytic Adenoviruses. Hum Gene Ther. 2006; 17: 929–40. [PubMed: 16972761]
30. Mosmann, T. J Immunol Methods. Vol. 65. Elsevier; 1983. Rapid colorimetric assay for cellular growth and survival: Application to proliferation and cytotoxicity assays; 55–63.
31. Lal S, Lacroix M, Tofilon P, Fuller GN, Sawaya R, Lang FF. An implantable guide-screw system for brain tumor studies in small animals. J Neurosurg. 2000. [PubMed: 10659021]
32. Studebaker, AW, Hutzen, B, Pierson, CR, Shaffer, TA, Raffel, C, Jackson, EM. Neuro Oncol. Vol. 17. Oxford University Press; 2015. Oncolytic measles virus efficacy in murine xenograft models of atypical teratoid rhabdoid tumors; 1568–77.
33. Abengozar-Muela M, Esparza MV, Garcia-Ros D, Vásquez CE, Echeveste JI, Idoate MA, et al. Diverse immune environments in human lung tuberculosis granulomas assessed by quantitative multiplexed immunofluorescence. Mod Pathol Mod Pathol. 2020. [PubMed: 32591586]
34. Martinez-Valbuena, I, Valenti-Azcarate, R, Amat-Villegas, I, Riverol, M, Marcilla, I, de Andrea, CE. , et al. Ann Neurol. Vol. 86. John Wiley and Sons Inc; 2019. Amylin as a potential link between type 2 diabetes and alzheimer disease; 539–51.
35. Bergelson, JM, Cunningham, JA, Droguett, G, Kurt-Jones, EA, Krithivas, A, Hong, JS. , et al. Science. Vol. 275. American Association for the Advancement of Science; 1997. Isolation of a common receptor for Coxsackie B viruses and adenoviruses 2 and 5; 1320–3.
36. Coyne, CB, Bergelson, JM. Adv Drug Deliv Rev. Vol. 57. Elsevier; 2005. CAR: A virus receptor within the tight junction; 869–82.
37. Spence, T, Perotti, C, Sin-Chan, P, Picard, D, Wu, W, Singh, A. , et al. Neuro Oncol. Vol. 16. Oxford University Press; 2014. A novel C19MC amplified cell line links Lin28/let-7 to mTOR signaling in embryonal tumor with multilayered rosettes; 62–71.
38. Obeid, M, Tesniere, A, Ghiringhelli, F, Fimia, GM, Apetoh, L, Perfettini, J-L. , et al. Nat Med. Vol. 13. Nature Publishing Group; 2007. Calreticulin exposure dictates the immunogenicity of cancer cell death; 54–61.
39. Buscariollo DL, Park HS, Roberts KB, Yu JB. Survival outcomes in atypical teratoid rhabdoid tumor for patients undergoing radiotherapy in a Surveillance, Epidemiology, and End Results analysis. Cancer. 2012; 118: 4212–9. [PubMed: 22213196]
40. Jiang H, Clise-Dwyer K, Ruisaard KE, Fan X, Tian W, Gumin J, et al. Delta-24-RGD oncolytic adenovirus elicits anti-glioma immunity in an immunocompetent mouse model. PLoS One. 2014; May 16. 9 e97407 doi: 10.1371/journal.pone.0097407 [PubMed: 24827739]
41. Billerbeck, E, Barry, WT, Mu, K, Dorner, M, Rice, CM, Ploss, A. Blood. Vol. 117. American Society of Hematology; 2011. Development of human CD4+FoxP3+ regulatory T cells in human stem cell factor-, granulocyte-macrophage colony-stimulating factor-, and interleukin-3-expressing NOD-SCID IL2Rγnull humanized mice; 3076–86.

42. Li, M, Lee, KF, Lu, Y, Clarke, I, Shih, D, Eberhart, C. , et al. Cancer Cell. Vol. 16. Cell Press; 2009. Frequent Amplification of a chr19q13.41 MicroRNA Polycistron in Aggressive Primitive Neuroectodermal Brain Tumors; 533–46.
43. Johann, PD, Erkek, S, Zapatka, M, Kerl, K, Buchhalter, I, Hovestadt, V. , et al. Cancer Cell. Vol. 29. Cell Press; 2016. Atypical Teratoid/Rhabdoid Tumors Are Comprised of Three Epigenetic Subgroups with Distinct Enhancer Landscapes; 379–93.
44. Li, M, Lockwood, W, Zielenska, M, Northcott, P, Ra, YS, Bouffet, E. , et al. Cancer Genet. Vol. 205. Elsevier; 2012. Multiple CDK/CYCLIND genes are amplified in medulloblastoma and supratentorial primitive neuroectodermal brain tumor; 220–31.
45. Picard D, Miller S, Hawkins CE, Bouffet E, Rogers HA, Chan TSY, et al. Markers of survival and metastatic potential in childhood CNS primitive neuro-ectodermal brain tumours: An integrative genomic analysis. Lancet Oncol. 2012; 13: 838–48. DOI: 10.1016/S1470-2045(12)70257-7 [PubMed: 22691720]
46. Lee, RS, Stewart, C, Carter, SL, Ambrogio, L, Cibulskis, K, Sougnez, C. , et al. J Clin Invest. Vol. 122. American Society for Clinical Investigation; 2012. A remarkably simple genome underlies highly malignant pediatric rhabdoid cancers; 2983–8.
47. Kieran, MW, Roberts, CWM, Chi, SN, Ligon, KL, Rich, BE, MacConaill, LE. , et al. Pediatr Blood Cancer. Vol. 59. John Wiley & Sons, Ltd; 2012. Absence of oncogenic canonical pathway mutations in aggressive pediatric rhabdoid tumors; 1155–7.
48. Friedman GK, Moore BP, Nan L, Kelly VM, Etminan T, Langford CP, et al. Pediatric medulloblastoma xenografts including molecular subgroup 3 and CD133+ and CD15+ cells are sensitive to killing by oncolytic herpes simplex viruses. Neuro Oncol. 2016; 18: 227–35. DOI: 10.1093/neuonc/nov123 [PubMed: 26188016]
49. Lal S, Carrera D, Phillips JJ, Weiss WA, Raffel C. An oncolytic measles virus-sensitive Group 3 medulloblastoma model in immune-competent mice. Neuro Oncol. 2018; 20: 1606–15. DOI: 10.1093/neuonc/noy089 [PubMed: 29912438]
50. Studebaker, AW, Hutzen, BJ, Pierson, CR, Haworth, KB, Cripe, TP, Jackson, EM. , et al. Mol Ther - Oncolytics. Vol. 6. American Society of Gene and Cell Therapy; 2017. Oncolytic Herpes Virus rRp450 Shows Efficacy in Orthotopic Xenograft Group 3/4 Medulloblastomas and Atypical Teratoid/Rhabdoid Tumors; 22–30.
51. Varela-Guruceaga, M, Tejada-Solís, S, García-Moure, M, Fueyo, J, Gomez-Manzano, C, Patiño-García, A. , et al. Cancers (Basel). Vol. 10. Multidisciplinary Digital Publishing Institute; 2018. Oncolytic viruses as therapeutic tools for pediatric brain tumors; 226
52. Studebaker AW, Hutzen B, Pierson CR, Shaffer TA, Raffel C, Jackson EM. Oncolytic measles virus efficacy in murine xenograft models of atypical teratoid rhabdoid tumors. Neuro Oncol. 2015; 17: 1568–77. [PubMed: 25838138]
53. Garcia-Moure M, Martinez-Velez N, Gonzalez-Huarriz M, Marrodán L, Cascallo M, Alemany R, et al. The oncolytic adenovirus VCN-01 promotes anti-tumor effect in primitive neuroectodermal tumor models. Sci Rep. 2019; 9: 1–10. DOI: 10.1038/s41598-019-51014-1 [PubMed: 30626917]
54. Glass, R, Synowitz, M. Acta Neuropathol. Springer Verlag; 2014. CNS macrophages and peripheral myeloid cells in brain tumours; 347–62.
55. Melcher, V, Graf, M, Interlandi, M, Moreno, N, de Faria, FW, Kim, SN. , et al. Acta Neuropathol. Vol. 139. Springer; 2020. Macrophage-tumor cell interaction promotes ATRT progression and chemoresistance; 913–36.
56. Jogler C, Hoffmann D, Theegarten D, Grunwald T, Uberla K, Wildner O. Replication properties of human adenovirus in vivo and in cultures of primary cells from different animal species. J Virol. 2006; Mar 16. 80: 3549–58. doi: 10.1128/JVI.80.7.3549-3558.2006 [PubMed: 16537623]
57. Beckmann PJ, Larson JD, Larsson AT, Ostergaard JP, Wagner S, Rahrmann EP, et al. Sleeping beauty insertional mutagenesis reveals important genetic drivers of central nervous system embryonal tumors. Cancer Res. 2019; 79: 905–17. DOI: 10.1158/0008-5472.CAN-18-1261 [PubMed: 30674530]
58. Ng, JMY, Martinez, D, Marsh, ED, Zhang, Z, Rappaport, E, Santi, M. , et al. Cancer Res. Vol. 75. American Association for Cancer Research; 2015. Generation of a mouse model of atypical

teratoid/rhabdoid tumor of the central nervous system through combined deletion of Snf5 and p53; 4629–39.

59. Neumann JE, Wefers AK, Lambo S, Bianchi E, Bockstaller M, Dorostkar MM, et al. A mouse model for embryonal tumors with multilayered rosettes uncovers the therapeutic potential of Sonic-hedgehog inhibitors. Nat Med. 2017; 23: 1191–202. [PubMed: 28892064]

Europe PMC Funders Author Manuscripts

Europe PMC Funders Author Manuscripts

Translational relevance

AT/RTs and CNS-PNETs are pediatric brain tumors with few therapeutic options at recurrence and a poor survival rate. Moreover, patients who survive face severe side effects that hinder their quality of life. Advancements in the treatment of these rare tumors have been hampered by the paucity of translational studies in relevant pediatric models that support their translation to clinical studies. Delta-24-RGD is an oncolytic adenovirus that has been shown to be safe and efficacious in adult brain tumors, offering a rationale for assessing its potential for childhood brain cancer treatment. In this study, we provide comprehensive evidence of the safety and efficacy of the oncolytic adenovirus Delta-24-RGD in animal models that recapitulate relevant challenging clinical problems of AT/RTs and CNS-PNETs, underscoring the therapeutic potential of this virus. Our data provide a strong foundation for initiating a clinical trial implementing Delta-24-RGD for the treatment of these pediatric brain tumors.

Europe PMC Funders Author Manuscripts

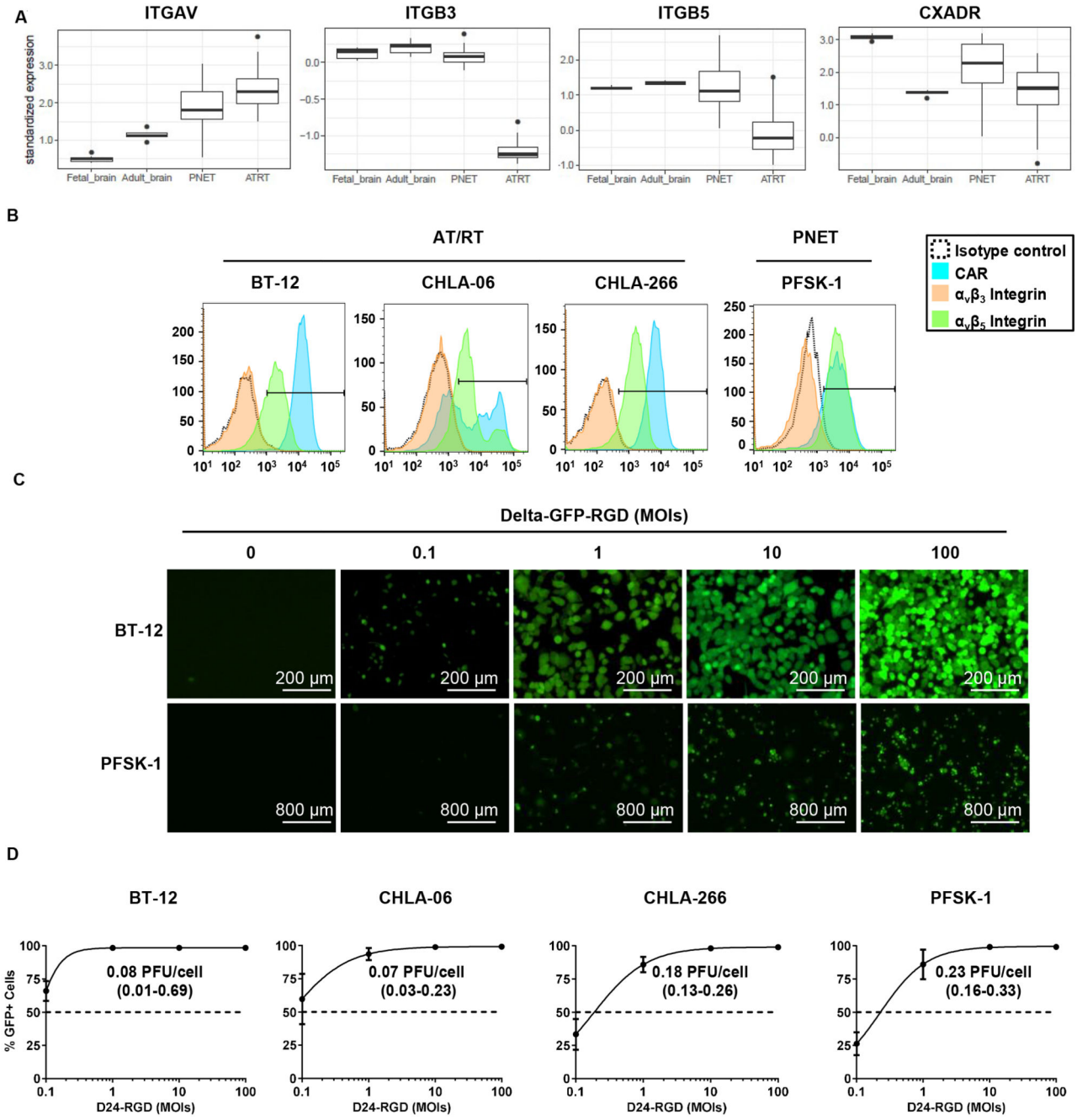

Fig. 1. Sensitivity of PNET and AT/RT cultures to Delta-24-RGD infection *in vitro*.

(**A**) Boxplot showing mRNA levels of the Delta-24-RGD receptors α_v (*ITGAV*), β_3 (*ITGB3*), and β_5 (*ITGB5*) integrins and CAR (*CXADR*) in fetal and adult brain samples and PNET and AT/RT tumor biopsies. (**B**) Flow cytometry histograms of the expression levels of the adenoviral receptors $\alpha_v\beta_3$ integrin, $\alpha_v\beta_5$ integrin, and CAR in the AT/RT cell lines BT-12, CHLA-06, and CHLA-266 and the PNET cell line PFSK-1. Black lines indicate the fluorescence threshold to identify positive cells. (**C**) Representative fluorescence images of BT-12 and CHLA-06 cell lines at 48 h after infection with Delta-24-RGD-GFP at

different MOIs ranging from 0 to 100 PFUs/cell. (**D**) Infectivity of Delta-24-RGD in BT-12, CHLA-06, CHLA-266, and PFSK-1 cells measured by flow cytometry as the percentage of GFP+ cells at 48 h after infection with Delta-24-RGD-GFP at MOIs ranging from 0.1 to 100 PFUs/cell. Dots represent the mean GFP+ cells ± SD (n=3), and values indicate the MOI needed to infect 50% of the culture (95% c.i.).

Europe PMC Funders Author Manuscripts

Europe PMC Funders Author Manuscripts

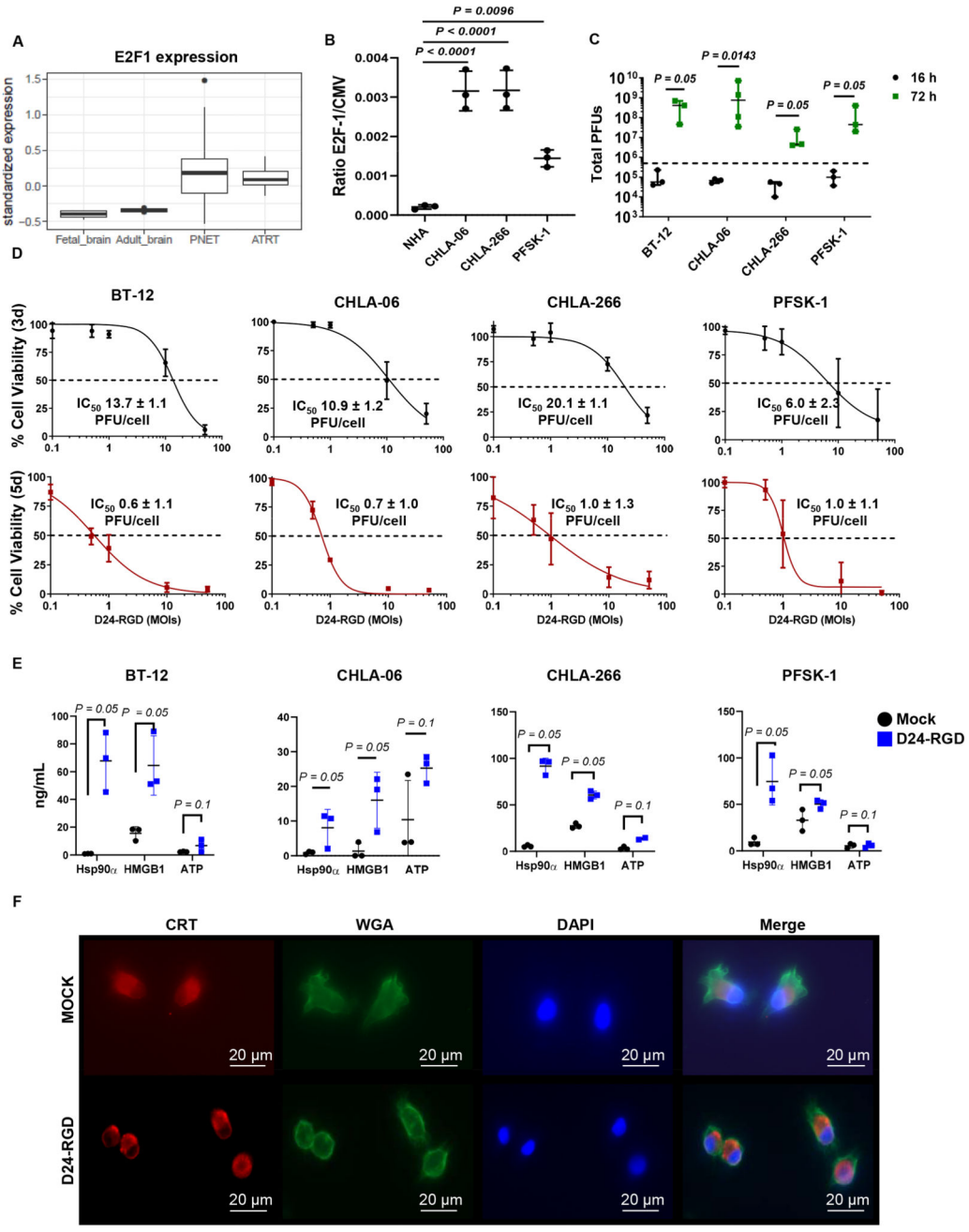

Fig. 2. Delta-24-RGD replication in AT/RT and PNET cultures mediates tumor cell death and DAMP release *in vitro*.

(**A**) Boxplot showing the mRNA levels of E2F-1 in fetal and adult brain samples and PNET and AT/RT tumor biopsies. (**B**) Measurement of E2F-1 transcription factor activation in normal human astrocytes (NHAs) and AT/RT (CHLA-06 and CHLA-266) and PNET (PFSK-1) cultures. Values are indicated as the ratio of E2F-1/CMV reporter signals (mean ± SD; n=3; one-way ANOVA; *P<0.0001*). (**C**) Total viral infectious titers (PFUs) measured in BT-12, CHLA-06, CHLA-266, and PFSK-1 cultures at 16 (black) and 72 h (green)

after infection with Delta-24-RGD at an MOI of 10. Dashed lines indicate the total initial viral input ($5x10^5$ PFUs). Dots specify viral titers for each experimental replicate, and bars represent the median viral titer ± 95% confidence interval (c.i.) (n=3/4; one-tailed Mann-Whitney test). (**D**) MTS assays to determine the percentages of viable BT-12, CHLA-06, CHLA-266, and PFSK-1 cells at three days (black graphs) or five days (red graphs) after infection with Delta-24-RGD at 0.1, 0.5, 1, 10, or 50 PFUs/cell. Dots indicate the percentages of viable cells in infected cultures compared to those in noninfected cultures (mean ± SD, n=3), and values indicate the mean IC_{50} ± SD (n=3). (**E**) Concentrations of the damage-associated molecular patterns (DAMPs) Hsp90α, HMGB1, and ATP in supernatants obtained from BT-12, CHLA-06, CHLA-266, and PFSK-1 cultures at 72 h after infection with Delta-24-RGD at the corresponding IC_{50} values for each group or after mock infection. Bar graphs indicate the mean ± SD (n=3; one-tailed Mann-Whitney test). (**F**) Representative fluorescence microscopy images of CHLA-06 cultures at 4 h after infection with Delta24-RGD or mock infection. Calreticulin (CRT) at the cell surface was detected by immunofluorescence (red). Cell membranes (green) and nuclei (blue) were counterstained with wheat germ agglutinin (WGA) and DAPI, respectively.

Europe PMC Funders Author Manuscripts

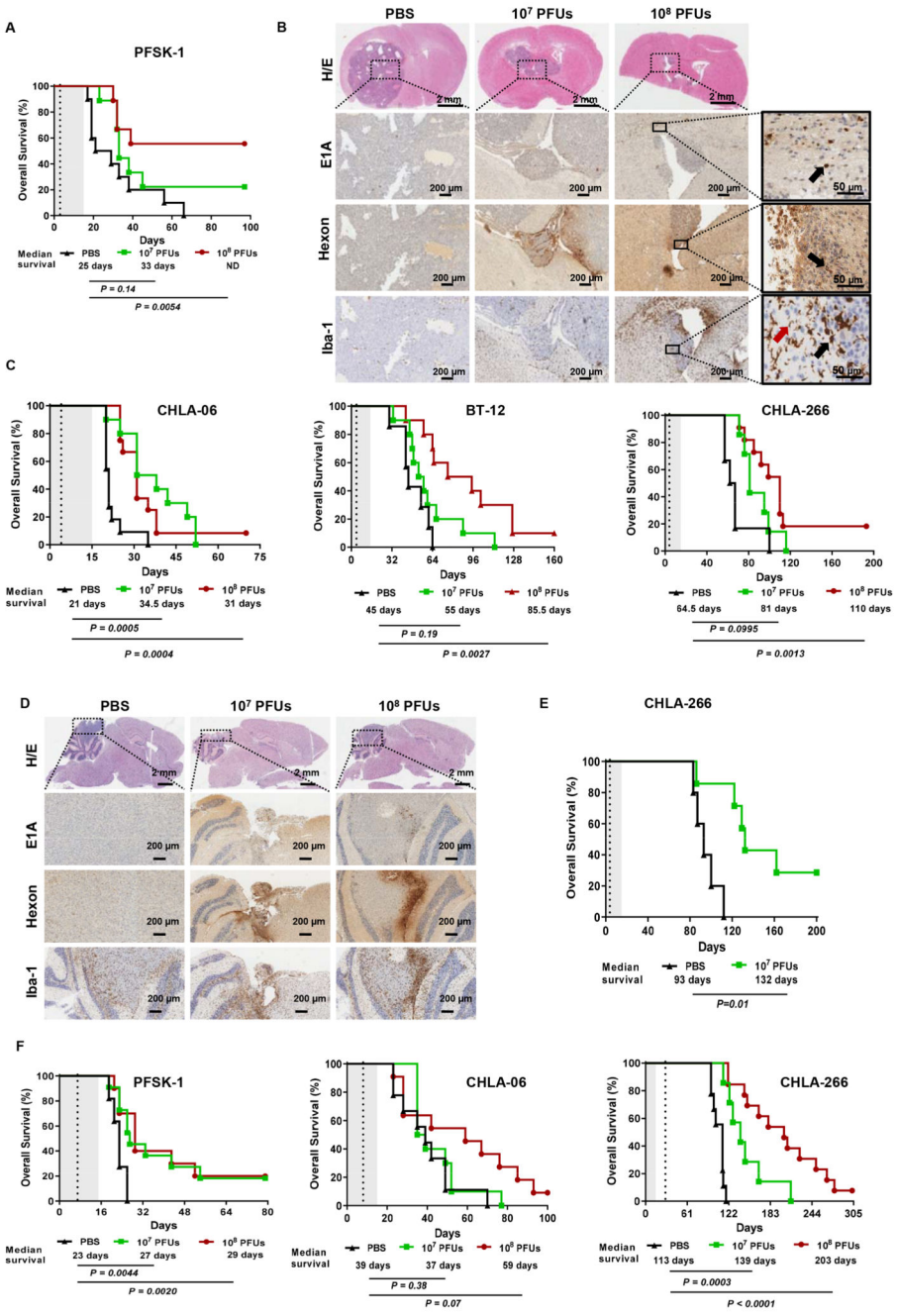

Fig. 3. Administration of Delta-24-RGD extends the overall survival of early and advanced PNET and AT/RT mouse models.

(**A**) Survival curve comparisons between mice bearing supratentorial PFSK-1 tumors that were either mock treated (PBS) or treated with 10^7 or 10^8 PFUs of Delta-24-RGD (*P<0.022*; log-rank test). The table below the survival graph contains the median survival and significance of comparisons between the 10^7 or 10^8 PFU-treated group and the mock-treated group. The dashed vertical line indicates administration of the virus. (**B**) Representative images of mice bearing supratentorial PFSK-1 tumors at 14 days after treatment with PBS

Europe PMC Funders Author Manuscripts

or 10^7 or 10^8 PFUs of Delta-24-RGD. Tumors were stained with hematoxylin/eosin (H/E) and immunostained for the adenoviral proteins E1A and hexon as well as the microglial marker Iba-1. The magnification at the bottom-right corner has been included to illustrate differential morphology between resting stellar-shaped microglia (red arrow) and activated amoeboid microglia (black arrow). (**C**) Survival curve comparisons (log-rank test) between mice bearing infratentorial (cerebellar) CHLA-06, BT-12 and CHLA-266 tumors that were mock treated (PBS) or treated with 10^7 or 10^8 PFUs of Delta-24-RGD. The table below the survival graph contains the median survival and significance of comparisons between the 10^7 or 10^8 PFU-treated group and the mock-treated group. (**D**) Representative images of CHLA-06 tumors at 14 days after treatment with PBS or 10^7 PFUs or 10^8 PFUs of Delta-24-RGD. Tumors were stained with H/E and immunostained for the adenoviral proteins E1A and hexon as well as the microglial marker Iba-1. (**E**) Survival curve comparisons (log-rank test) between mice bearing supratentorial CHLA-266 tumors that were mock treated (PBS) or treated with 10^7 PFUs of Delta-24-RGD. The table below the survival graph contains the median survival and significance of the comparison between the 10^7 PFU-treated group and the mock-treated group. Dashed vertical lines in survival plots indicate administration of Delta-24-RGD. (**F**) Survival curves and comparisons (log-rank test) in different tumor models that were either mock treated with PBS or treated with Delta-24-RGD (10^7 and 10^8 PFUs). In supratentorial PNET experiments, PFSK-1 tumors were treated on day 7, infratentorial CHLA-06 AT/RTs were treated on day 8, and supratentorial CHLA-266 AT/RTs were treated on day 29. The table below the survival graph contains the median survival and significance of comparisons between the 10^7 PFU-treated group and the mock-treated group. Dashed vertical lines in survival plots indicate administration of Delta-24-RGD.

Europe PMC Funders Author Manuscripts

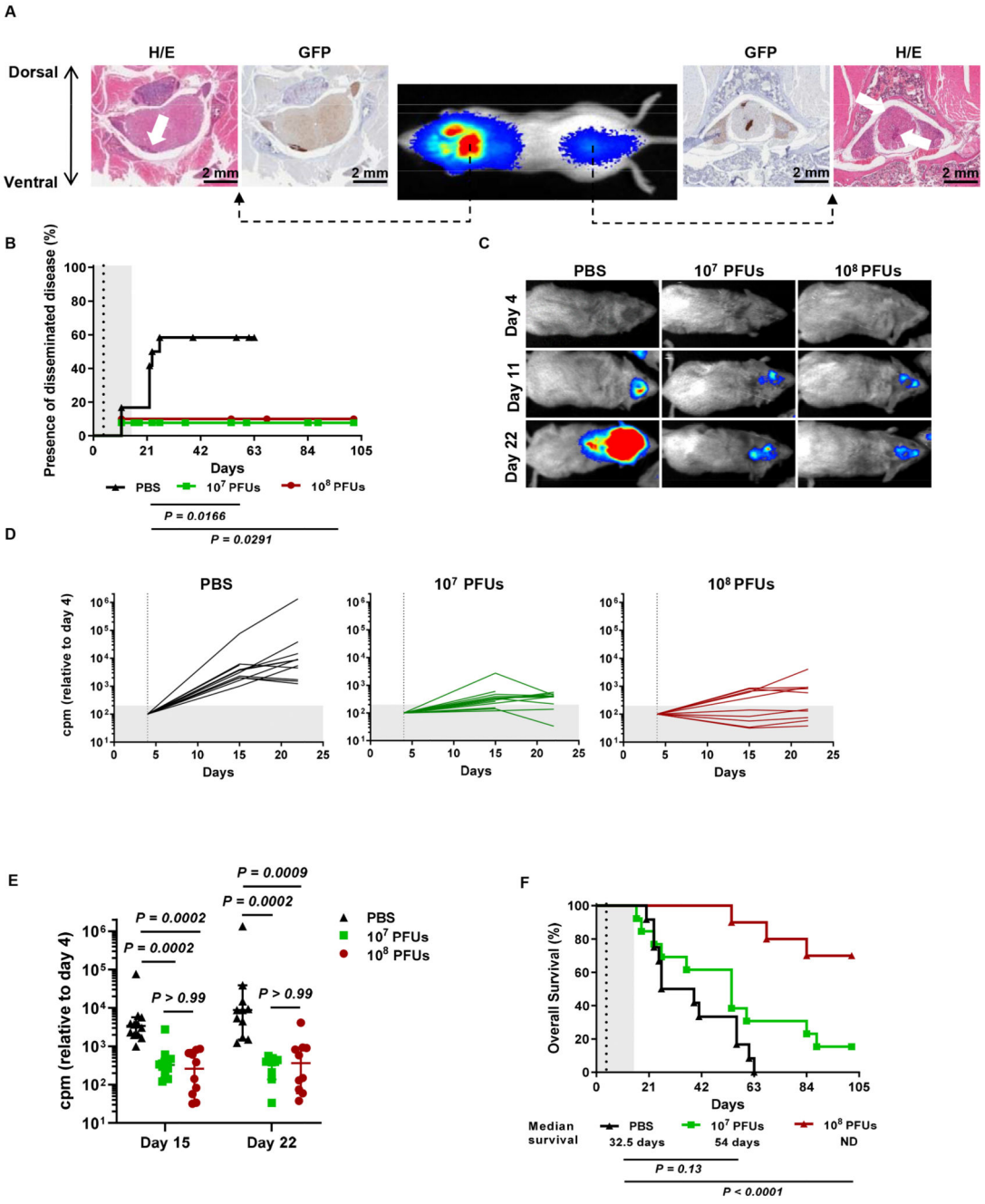

Fig. 4. Delta-24-RGD hinders the development of disseminated AT/RT lesions.

(A) Representative bioluminescence images of mice at 21 days after intraventricular administration of BT-12-luc/GFP cells showing the presence of luciferase signals at cranial and spinal locations. H/E and GFP staining demonstrated that the luciferase signals corresponded to local and disseminated tumor lesions. (**B**) Kaplan-Meier plot comparing the development of secondary AT/RT BT-12 tumors (log-rank test). Dots on the survival curves indicate death events. (**C**) Representative images of mice developing disseminated tumors acquired on days 4 (day of treatment), 11, and 22 after injection of BT-12-luc cells

into the right ventricle. (**D**) Evolution of tumor growth measured as luminometry signals in mice treated with 10^7 or 10^8 PFUs of Delta-24-RGD or mock treated with PBS. The total counts per minute (cpm) measured in whole mice were normalized to the intensity of the signal on the day of treatment (dashed vertical line). (**E**) Analysis of differences in tumor sizes among the three experimental groups at days 15 and 22 after injection of tumor cells. Each dot represents an individual value, and bars indicate the median cpm ± 95% c.i. (Kruskal-Wallis test, Dunn's correction). (**F**) Survival curve comparisons between mice bearing intraventricular BT-12 tumors that were mock treated (PBS) or treated with 10^7 or 10^8 PFUs of Delta-24-RGD (log-rank test). Dashed vertical lines in survival plots indicate administration of Delta-24-RGD.

Europe PMC Funders Author Manuscripts

Europe PMC Funders Author Manuscripts

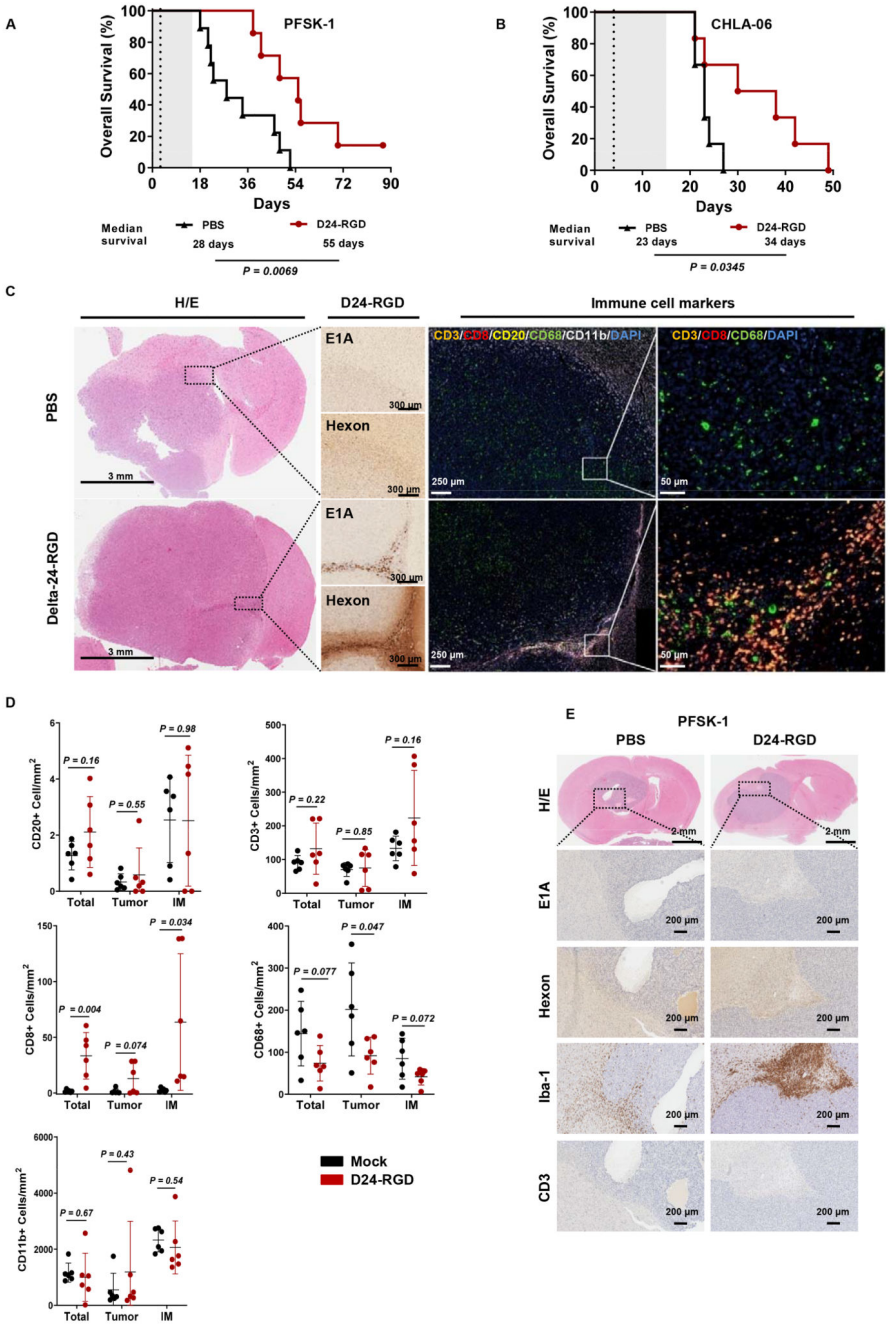

Fig. 5. Therapeutic effect of Delta-24-RGD on immunocompetent humanized mice.

(**A**) Survival curve comparisons (log-rank test) between Delta-24-RGD- and PBS-treated humanized mice bearing supratentorial PFSK-1 or (**B**) CHLA-06 tumors. Dashed vertical lines indicate administration of Delta-24-RGD. (**C**) Representative images of brain sections obtained from humanized mice bearing CHLA-06 tumors. Samples were stained with hematoxylin/eosin (H/E) and immunostained for the viral proteins E1A and hexon; furthermore, they were subjected to multiplexed immunofluorescence to detect the following immune cell markers: CD3 (orange), CD8 (red), CD20 (yellow), CD68 (green), and CD11b

(white). Nuclei were counterstained with DAPI (blue). (**D**) Quantification of immune cell populations identified by multiplexed immunofluorescence in the whole tumor (total), central tumor region (tumor), and invasive margin of the tumor (IM). Bars indicate the mean ± SD (n=6; each dot represents the mean stamps counted per mouse), and Student's t-tests were used for comparisons between PBS (black) and Delta-24-RGD (red) treatments in each region. (**E**) Representative histological staining images of brain sections from humanized mice bearing PFSK-1 tumors. Whole tumors were stained with H/E or immunostained for the viral proteins E1A and hexon and the immune cell markers Iba-1 and CD3.

Europe PMC Funders Author Manuscripts